A new process for the recovery of iron, vanadium, and titanium from vanadium titanomagnetite

by S.Y. Chen* and M.S. Chu*

Synopsis

A new process comprising metallizing reduction, magnetic separation, and electroheat melting separation is proposed with the aim of achieving high recoveries of iron, vanadium, and titanium from vanadium titanomagnetite. The effects of magnetic intensity, reduction temperature, reduction time, carbon ratio, and coal particle size on the efficiency of reduction-magnetic separation were investigated, the reaction mechanisms elucidated by SEM and EDS analysis, and the optimal process parameters established. Recoveries of up to 80.08% for titanium, 95.07% for iron, and 71.60% for vanadium were achieved.

The reduction sequence is shown to be: $Fe_2O_3 \rightarrow Fe_3O_4 \rightarrow FeO \rightarrow Fe$; $Fe_2TiO_5 \rightarrow Fe_2TiO_4 + TiO_2 \rightarrow Fe + FeTiO_3 \rightarrow Fe + FeTi_2O_5 \rightarrow Fe + TiO_2$.

Keywords
VTM, metallization reduction, magnetic separation, electrothermal smelting separation, phase transition.

Introduction

Vanadium titanomagnetite (VTM), which contains valuable elements such as iron, vanadium, and titanium, has an extremely high potential value. VTM resources in the PanXi regions of China are estimated at up to 10 Gt (billion tons), and account for 93% and 63% of the country's titanium and vanadium resources respectively. The exploitation of VTMs has thus received much attention (Barksdale, 1966; Chen *et al.*, 2011).

Owing to their poor grades, fine grain size, and complex mineralogy, VTMs are difficult to treat (Katsura and Kushiro, 1961; Akimoto and Katsura, 1959). In China, the main method of VTM utilization is in ironmaking via the blast furnace route and the basic oxygen furnace process for vanadium recovery. However, the recovery ratios of Fe (into pig iron), V (into vanadium slag), and Ti (into ilmenite) are only 70%, 42%, and 25% respectively, which are relatively low. Meanwhile, 70 Mt of high-titanium slag are discarded on the riversides of the Jinsha River, resulting in waste of resources and environmental pollution (Diao, 1999, Ma *et al.*, 2000). Many new processes have been recently proposed and studied both in China and abroad (Roshchin *et al.*, 2011; Wang *et al.*, 2008; Yuan *et al.*, 2006; Lei *et al.*, 2011), such as chemical extraction, direct reduction, and EAF smelting. However, none of the proposed processes have been shown to be commercially viable, owing to poor selectivity and recoveries, and economic efficiency.

In this paper, a new process for VTM beneficiation is proposed, comprising metallizing reduction, magnetic separation, and electroheat melting separation. The proposed flow sheet is shown in Figure 1. The VTM is firstly reduced by carbothermal reduction, and the titanium (non-magnetic fraction) and iron and vanadium (magnetic fraction) are separated by magnetic separation. The magnetic fraction bearing iron and vanadium is melted and separated by electrothermal smelting separation. The high-titanium slag in the non-magnetic fraction and vanadium slag could be further treated by a hydrometallurgical route.

Experimental methods

Materials

The VTM concentrate used in this investigation was obtained from the PanXI region in China. The chemical composition and size distribution of the VTM concentrate are shown in Table I. The VTM concentrate contained 53.91% total iron, 13.03% titanium oxide, and 0.52%. vanadium oxide.

The X-ray diffraction (XRD) patterns of VTM concentrate are shown in Figure 2. The main phases are titanomagnetite ($Fe_xTi_{3-x}O_4$), magnetite (Fe_3O_4), ilmenite ($FeTiO_3$), vanadium spinel ($FeO{\bullet}V_2O_3$), and augite [$(Mg,Fe,Al,Ti)(Ca,Mg,Fe)(Si,Al)_2O_4$].

* *School of Materials and Metallurgy, Northeastern University, China.*

 ISSN 2225-6253. Paper received Sep. 2013; revised paper received Nov. 2013.

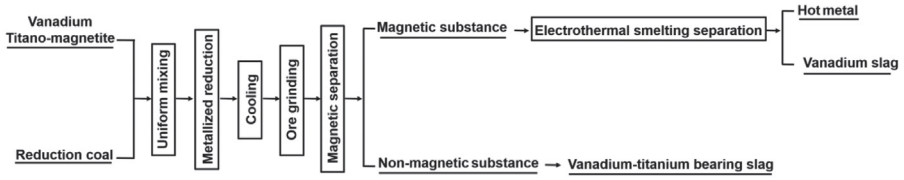

Figure 1—Flow chart of the new process

Table I

Chemical analysis of materials

Chemical composition of VTM		Size distribution of VTM	
Fe_{tot}	53.91%	< 40	27.93%
FeO	31.13%	40 ~ 74	18.95%
V_2O_5	0.52%	74 ~ 100	12.07%
TiO_2	13.03%	100 ~ 200	28.37%
CaO	0.68%	Coal chemical properties	
SiO_2	3.20%	Aad	4.29%
MgO	2.71%	Vdaf	33.64%
Al_2O_3	3.82%	Std	0.16%
-	-	FC	62.12%

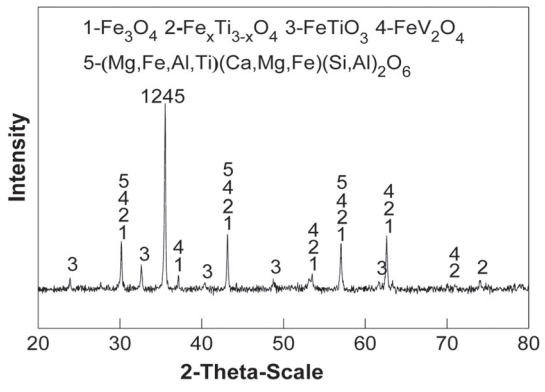

Figure 2—XRD pattern of VTM concentrate

Coal is used as reductant. The chemical analysis of the coal is listed in Table I, which shows that the coal is high in fixed carbon (FC), and low in ash (Aad) and total sulphur (Std).

Apparatus and procedure

Figure 3 shows the schematic diagram of the experiment procedure, which consists of three main steps.

The first step consists of metallization reduction. VTM concentrate (100 g) and coal were combined in mole ratios of fixed carbon to reducible oxygen (carbon ratio) of 0.8, 1.0, 1.2, 1.4, 1.6, and 1.8. The well-mixed sample was placed in a graphite crucible (Wang *et al.*, 2008) and reduced in a high-temperature laboratory furnace at various temperatures and times.

The crucible was removed from the furnace and allowed to cool. The reaction products were ground and a 10 g sample was placed in a DTCXG-ZN50 magnetic tube to separate the magnetic and non-magnetic fractions.

The magnetic fraction was then treated by electrothermal smelting. A 135 g sample of the magnetic concentrate was dried for 3 hours at 105°C, then mixed with 0.9 g of coal, placed in a high-purity graphite crucible, and heated in a high-temperature resistance furnace at 1550°C for 120 minutes to separate a metallic iron phase and a vanadium slag.

The chemical compositions of the metallization reduction product, the magnetic and non-magnetic fractions, and the iron phase and vanadium slag were analysed by X-ray diffraction XRD and scanning electron microscopy (SEM) to investigate the effects of process conditions and the reaction mechanisms.

Results and discussion

Effect of magnetic intensity

The finely ground metallization-reduction product was separated in the DTCXG-ZN50 magnetic tube at magnetic intensities from 25 mT to 125 mT. The process parameters for the metallization-reduction step were: reduction temperature 1350°C, reduction time 30 minutes, carbon ratio 1.0, coal particle size -74 μm.

The chemical composition and metallization rate of the reduction product are listed in Table II, and the effects of magnetic intensity on the metallizing reduction and magnetic separation indexes are shown in Figure 4. The result shows that titanium partitions into the high-titanium slag phase of

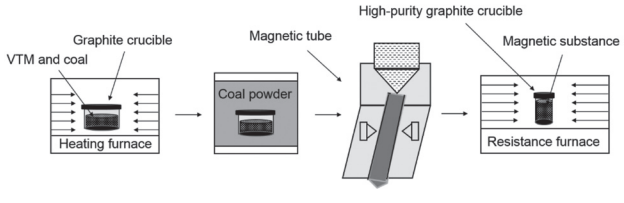

Figure 3—Schematic diagram of experiment procedure and equipment

Table II

Chemical composition and metallization rate of reduction product

Fe_{tot}	65.59 %
MFe	61.84 %
V_2O_5	0.728 %
TiO_2	16.5 %
Metallization	94.28 %

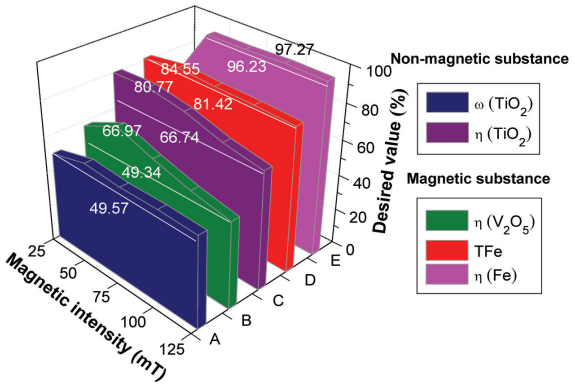

Figure 4—Effects of magnetic intensity on metallizing reduction and magnetic separation indexes

the non-magnetic fraction while iron and vanadium partition into the iron phase of the magnetic fraction. As shown in Figure 4, all of the process indexes, including titanium content ($\omega(TiO_2)$), recovery ratio of titanium ($\eta(TiO_2)$) in the non-magnetic fraction, recovery ratio of vanadium ($\eta(V_2O_5)$), iron content ($\omega(TFe)$), and recovery ratio of iron ($\eta(Fe)$) in the magnetic fraction, increase with increasing magnetic intensity from 25 mT to 50 mT, but show a downtrend trend as the magnetic intensity is increased beyond 50 mT. An optimal magnetic intensity of 50 mT was therefore selected for the subsequent experiments.

The reaction mechanisms were investigated based on SEM and energy dispersive spectrometry (EDS) of the reduction product (Figure 5). Figure 5(a) shows that the dispersed iron particles agglomerate due to metallizing reduction and carburization. Figures 5(a) and 5(b) show that the high-titanium slag phase (gray phase) becomes entrained in the iron phase (white phase) on account of excessive magnetic force, leading to the decrease of $\eta(Fe)$, $\eta(V_2O_5)$, and $\eta(TiO_2)$.

Effect of reduction temperature

To determine the optimum reduction temperature, a series of metallizing reduction and magnetic separation tests were carried out at reduction temperature of 1250°C,1275°C, 1300°C, 1325°C, and 1350°C. The other process parameters were kept constant as follows: reduction time 30 minutes, carbon ratio 1.0, coal particle size -74 μm, magnetic intensity 50 mT. The effects of reduction temperature on metallization rate and the iron content are shown in Figure 6. The $\omega(TFe)$) and metallization rate of the reduction product increase gradually with increasing reduction temperature. At a reduction temperature of 1350°C, the $\omega(TFe)$ and metallization rate are 65.59% and 94.28%, respectively.

The effects of reduction temperature on the metallizing reduction and magnetic separation indexes are shown in Figure 7. The $\omega(TiO_2)$ and $\eta(TiO_2)$ of the non-magnetic fraction increase from 26.43% to 54.73% and from 62.58% to 80.77% respectively. The $\omega(TFe)$, $\eta(Fe)$, and $\eta(V_2O_5)$ of the magnetic fraction also increase, from 78.94% to 84.55%, from 75.58% to 96.23%, and from 44.54% to 66.97% respectively with the reduction temperature increasing from 1250°C to 1350°C. Considering the heating capacity of the reduction equipment and the high recoveries of iron, vanadium, and titanium, an optimum reduction temperature of 1350°C was selected for the subsequent experiments.

Figure 8 shows that the reducibility of the iron-bearing phase in the reduction product is significantly improved by increasing the reduction temperature. Aggregation and growth of the iron particles is also facilitated and much larger iron particles are formed. As shown in Figure 8(e)-(f), the iron phase (A) can be separated from the high-titanium slag phase (B) by magnetic separation.

Effects of reduction time

To determine the optimum reduction time, a series of metallizing reduction and magnetic separation tests were carried out at reduction times of 10, 20, 30, 40, 50, and 60 minutes. The other process parameters were kept constant as follows: reduction temperature 1350°C, carbon ratio 1.0, coal particle size -74 μm, magnetic intensity 50 mT. The effects of reduction time on metallization and the iron content are

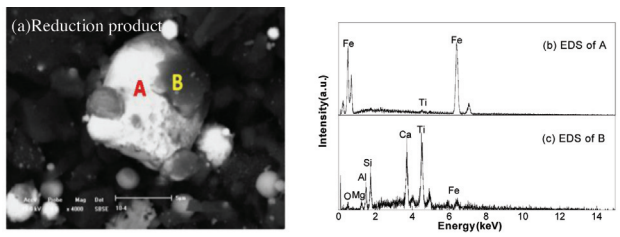

Figure 5—SEM and EDS images of the reduction product

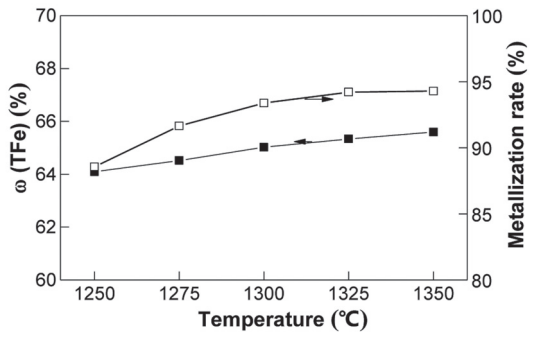

Figure 6—Effects of temperature on the reduction product

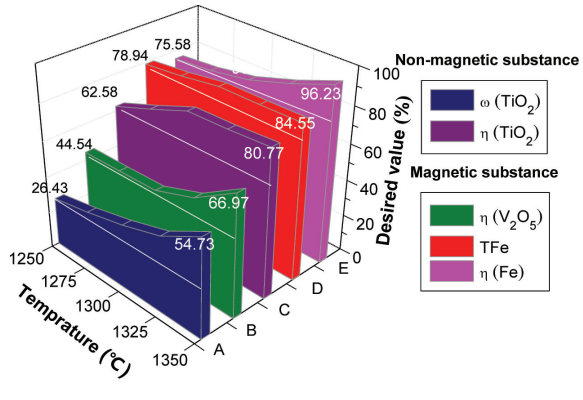

Figure 7—Effects of reduction temperature on the new process

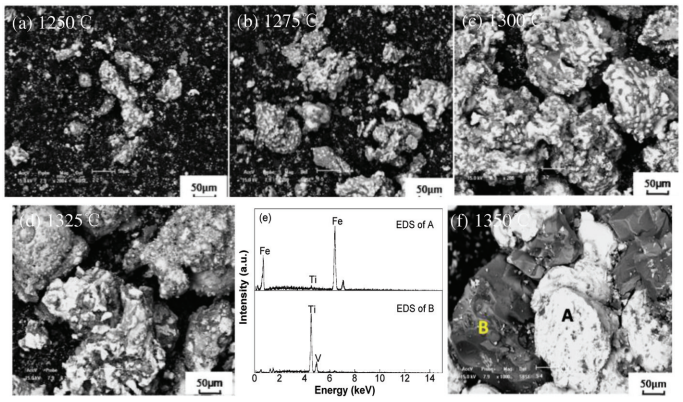

Figure 8—SEM image of reduction product at different reduction temperature

shown in Figure 9. The ω(TFe)) and metallization of the reduction product show a upward trend. At the maximum reduction time of 60 minutes, the ω(TFe) and metallization are 68.60% and 95.93%, respectively.

The effects of reduction time on metallizing reduction and magnetic separation indexes are shown in Figure 10. With increasing reduction time from 10 minutes to 60 minutes, the (TiO_2) and η(TiO_2) of the non-magnetic fraction increase from 18.33% to 55.39% and from 79.81% to 80.08% respectively. The ω(TFe), η(Fe), and η(V_2O_5) of the magnetic fraction also increase, from 74.82% to 86.56%, from 39.74% to 97.48%, and from 29.22% to 75.68%. An optimum reduction time of 60 minutes was therefore selected for the subsequent experiments.

The SEM micrographs of the six reduction products are shown in Figure 11. With increasing reduction time, the bearing-iron (white) phase aggregates and grows owing to the ongoing reduction reaction between VTM and coal. At the same time, iron-iron bonds form instead of iron-titanium bonds, accelerating the separation of the iron phase from the other phases.

Effects of carbon ratio

In test work to optimize the carbon ratio, the VTM and coal mixtures were prepared with carbon ratios of 0.8, 1.0, 1.2, 1.4, 1.6, and 1.8. The other process parameters were kept constant as follows: reduction temperature 1350°C, reduction time 60 minutes, coal particle size -74 μm, and magnetic

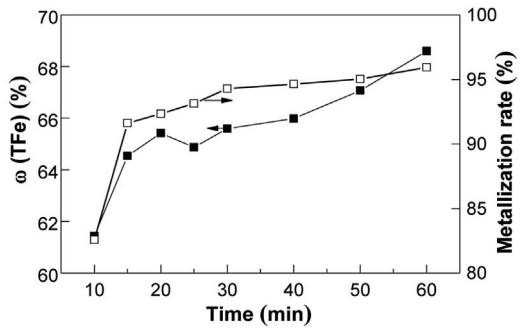

Figure 9—Effects of reduction time on the reduction product

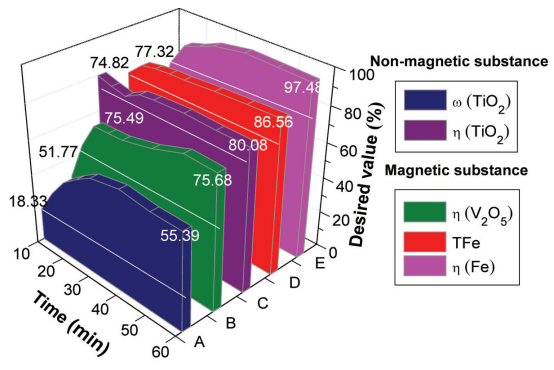

Figure 10—Effects of reduction time

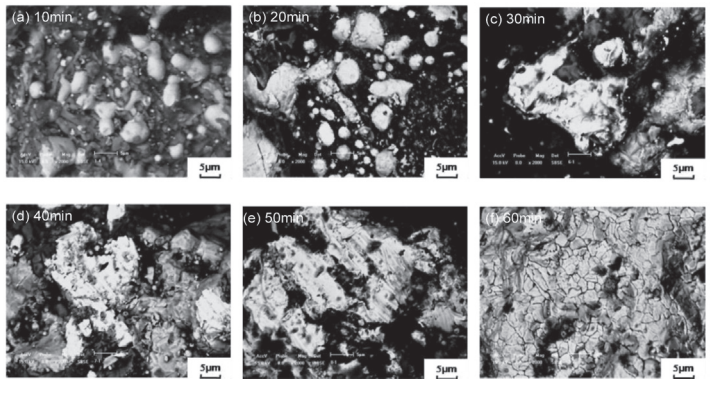

Figure 11—SEM images of reduction product with different reduction time

intensity 50 mT. The effects of carbon ratio on the metallization and iron content are shown in Figure 12. The metallization of the reduction product increases as the carbon ratio increases from 0.8, to 1.0, and then decreases as carbon ratios above 1.0.

The effects of carbon ratio on the metallizing reduction and magnetic separation indexes are shown in Figure 13. With the carbon ratio increasing from 0.8 to 1.0, the $\omega(TiO_2)$ and $\eta(TiO_2)$ of the non-magnetic fraction increase from 37.84% to 55.39% and from 76.07% to 80.08% respectively, and ω(TFe), η(Fe), and $\eta(V_2O_5)$ of the magnetic fraction increase from 83.81 % to 86.56 %, from 80.68 % to 97.48 %, and from 64.00 % to 75.68 %, respectively. With further increases in the carbon ratio from 1.0 to 1.8, the $\omega(TiO_2)$, ω(TFe), η(Fe), and $\eta(V_2O_5)$ show a downward trend. Taking into account the economics of the new process and effective utilization of resources and energy, the an optimum carbon ratio of around 1.0 was selected for metallizing reduction and magnetic separation.

The SEM micrographs of the reduction products obtained with different carbon ratios are shown in Figure 14. It can be seen that with an increase in the carbon ratio from 0.8 to 1.0, more iron particles (white) formed, aggregated, and grew, and a large number of bigger iron particles appeared to be separating the iron phase from the other phases. With further increases in the carbon ratio from 1.0, 1.4 to 1.8, the carbon is in excess, and the aggregation of reduced iron particles is hindered by superfluous graphitized carbon.

Effects of coal particle size

To determine the effects of coal particle size on the metallizing reduction and magnetic separation indexes, a series of reduction and magnetic separation tests were performed at coal particle sizes of -74 μm, -0.5 mm, -1 mm, -1.5 mm, and -2 mm. The other parameters were kept constant as follows: reduction temperature 1350°C, reduction time 60 minutes, carbon ratio 1.0, and magnetic intensity 50 mT. The effects of coal particle size on metallization and the iron content are shown in Figure 15. The ω(TFe)) and metallization of the reduction product show a downward trend with increasing coal size. When the coal particle size increased from -74 μm to -2 mm, the ω(TFe) and metallization decreased significantly from 68.60% to 60.07%, and from 95.93% to 85.73%, respectively.

The effects of coal particle size on the metallizing reduction and magnetic separation indexes are shown in Figure 16. Increasing in coal size from -74 μm to -2 mm had no significant effect on the $\eta(TiO_2)$ of the non-magnetic fraction. The ω(TFe), η(Fe), and $\eta(V_2O_5)$ of the magnetic fraction gradually decreased from 85.56% to 78.13%, from 97.48% to 75.57% and from 75.68% to 56.82 %, respectively. Thus, the optimum coal particle size for metallizing reduction and magnetic separation should be -74 μm.

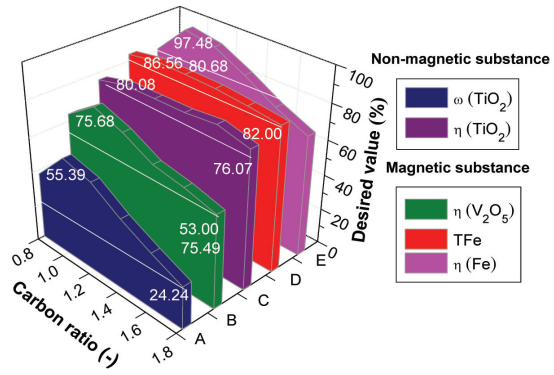

Figure 13—Effects of carbon ratio

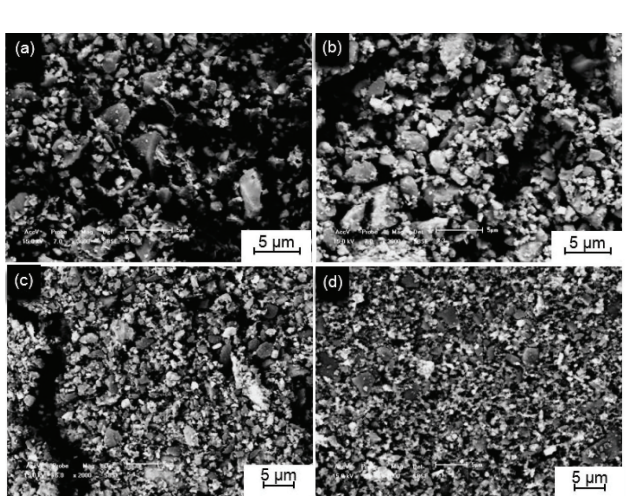

Figure 14—SEM and EDS photos of reduction product with different carbon ratios

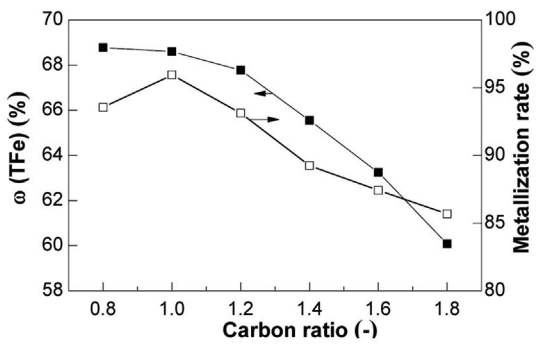

Figure 12—Effects of carbon ratio on the reduction product

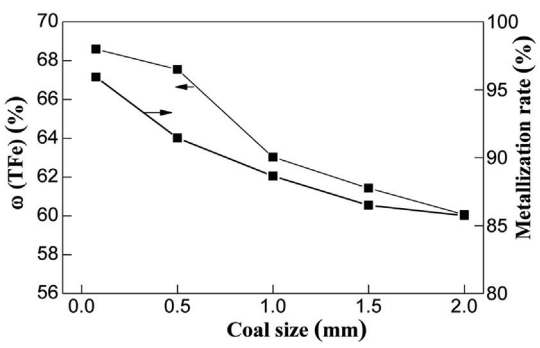

Figure 15—Effects of coal size on the reduction product

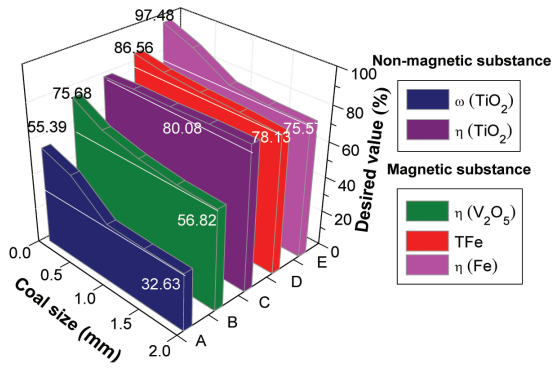

Figure 16—Effects of coal particle size index

Results and analysis of electrothermal smelting experiment

The chemical analyses of the magnetic (7.71 g) and non-magnetic substance (2.21 g) fractions obtained by magnetic separation are shown in Table III. The chemical compositions of the iron and vanadium-bearing slag obtained by electrothermal smelting are analysed and listed in Table IV. The results show that 97.53% of the iron partitions to the iron phase and 94.61% of the vanadium to the vanadium-bearing slag. Considering together the results of the metallizing reduction, magnetic separation, and electrothermal smelting separation experiments, the $\eta(TiO_2)$ of the non-magnetic fraction is 80.08%, and the η(Fe) in the iron phase and $\eta(V_2O_5)$ of the vanadium-bearing slag are 95.07% and 71.60%, respectively.

Thermodynamic analysis of the metallization reduction

All possible chemical reactions between VTM and coal are depicted in Figure 17. The standard Gibbs free energies ($\Delta G°$) of solid reactions and the gas-solid equilibrium of VTM reduced by CO are also shown.

As depicted in Figure 17, the solid reactions take place at first, and are then restricted by solid diffusion and interface reactions. At the same time, the gas–solid reactions taking place are greatly accelerated by the increasing CO partial pressure. For the thermodynamic analysis, it can be seen that the $\Delta G°$ values for all solid-solid and gas-solid reactions are negative at 1350°C, therefore the reduction reaction of VTM can proceed and the reduction products of iron oxide and ilmenite are iron and titanium oxides of low valences (Sadykhov *et al.*, 2010; Paunova, 2002).

Element migration process during metallization reduction

In order to illustrate the element migration process based on the optimum conditions, including reduction temperature of 1350°C, carbon ratio of 1.0, and coal particle size of less than 74 μm, the XRD patterns and phase compositions of the reduction product at different stages of reduction are given in Figure 18 and Table V (Pogudin *et al.*, 2010; Welham, 1996).

The main phases in the VTM concentrate are $Fe_xTi_{3-x}O_4$, Fe_3O_4, $FeTiO_3$, and augite. As reduction proceeds, Fe, FeO, and Fe_5TiO_8 appear (5 minutes); Fe_2TiO_5 appears and $FeTiO_3$ disappears (10 minutes); Fe_2TiO_4 and $FeTi_2O_5$ appear but FeO disappears (25 minutes); Fe_3O_4 and Fe_2TiO_4 disappear and $FeTiO_3$ appears (30 minutes); Fe_2TiO_5 disappears after 40 minutes, followed by $FeTiO_3$ after 50 minutes. Further increase in the reduction time to 60 minutes does not result in any further change in the phase composition, and the VTM is considered to be reduced completely. Considering the analyses of the thermodynamics and phase transition process, the reduction processes of iron oxide and ilmenite in VTM proceed as follows:

$$Fe_2O_3 \rightarrow Fe_3O_4 \rightarrow FeO \rightarrow Fe$$

$$Fe_2TiO_5 \rightarrow Fe_2TiO_4 + TiO_2 \rightarrow Fe + FeTiO_3 \rightarrow Fe + FeTi_2O_5 \rightarrow Fe + TiO_2$$

Conclusion

Based on the results obtained in this study, the following conclusions can be drawn.

Table III

Chemical composition of magnetic and non-magnetic fraction %

Constituent	Magnetic	Non-magnetic
Fe_{tot}	86.56	6.19
FeO	4.26	-
TiO_2	3.95	55.39
V_2O_5	0.649	0.667
CaO	0.22	1.90
SiO_2	1.18	13.01
MgO	1.72	6.77
Al_2O_3	1.16	11.50

Table IV

Chemical composition of iron and slag phase

Element	Iron phase	Slag phase
Mass	115.45 g	16.29 g
Fe_{tot}	98.72%	8.84%
V_2O_5	0.037%	5.39%
TiO_2	-	28.24%

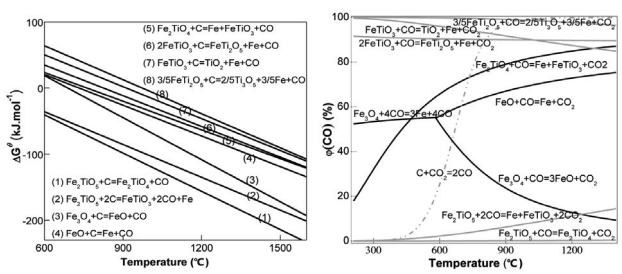

Figure 17—The results of thermodynamic analysis (after (Pesl and Eric, 2002; Huang, 2007)

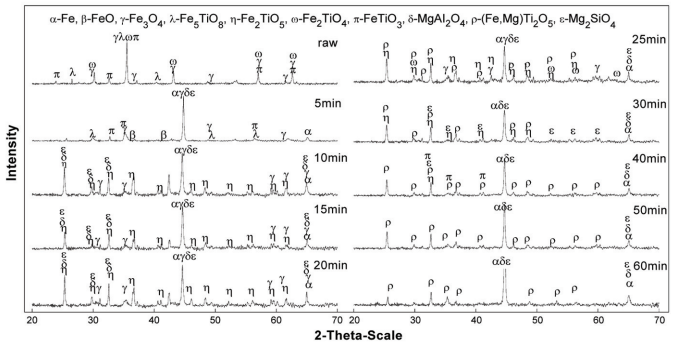

Figure 18—X-ray diffraction analysis of phase containing iron and titanium

Table V

Phase composition of reduction product with different reduction times

Time, min	Phase composition
0	Fe_3O_4, $FexTi_{3-x}O_4$, FeV_2O_4, $FeTiO_3$, augite
5	Fe, FeO, Fe_3O_4, Fe_5TiO_8, $FeTiO_3$, $MgAl_2O_4$
10	Fe, FeO, Fe_3O_4, Fe_2TiO_5, Fe_5TiO_8, $MgAl_2O_4$, $MgSi_2O_4$
15	Fe, FeO, Fe_3O_4, Fe_2TiO_5, $MgAl_2O_4$, $MgSi_2O_4$
20	Fe, FeO, Fe_3O_4, Fe_2TiO_5, $MgAl_2O_4$, $MgSi_2O_4$
25	Fe, Fe_3O_4, Fe_2TiO_5, Fe_2TiO_4, $MgAl_2O_4$, $MgSi_2O_4$
30	Fe, Fe_2TiO_5, $FeTiO_3$, $(Fe,Mg)Ti_2O_5$, $MgAl_2O_4$, $MgSi_2O_4$
40	Fe, $FeTiO_3$, $MgAl_2O_4$, $(Fe,Mg)Ti_2O_5$, $MgSi_2O_4$
50	Fe, $(Fe,Mg)Ti_2O_5$, $MgAl_2O_4$, $MgSi_2O_4$
60	Fe, $(Fe,Mg)Ti_2O_5$, $MgAl_2O_4$, $MgSi_2O_4$

The optimum process conditions for metallizing reduction and magnetic separation are a carbon ratio of 1.0, reduction temperature 1350°C, reduction time 60 minutes, magnetic intensity 50 mT, and coal particle size less than 74 μm. Under the above conditions, after electroheat melting separation of the magnetic fraction, the recovery ratio of titanium in the non-magnetic fraction is 80.08%, and recovery ratios of iron in molten iron and vanadium in molten slag are 95.07% and 71.60%, respectively.

Through the new process of metallizing reduction, magnetic separation, and electroheat melting separation, the effective separating of iron, vanadium and titanium in VTM could be achieved and iron in iron phase, vanadium in vanadium slag, and titanium in high titanium slag were successfully obtained.

Based on the analyses of the thermodynamics and phase transitions, the reduction of iron oxide and ilmenite in VTM proceeds as follows:

$$Fe_2O_3 \rightarrow Fe_3O_4 \rightarrow FeO \rightarrow Fe$$

$$Fe_2TiO_5 \rightarrow Fe_2TiO_4 + TiO_2 \rightarrow Fe+FeTiO_3 \rightarrow Fe + FeTi_2O_5 \rightarrow Fe + TiO_2$$

Acknowledgements

The research presented this paper was supported by National High-tech Research and Development Projects (Grant No. 2012AA062302) and Major Program of the National Natural Science Foundation of China (Grant No. 51090384). The work was also supported by the Fundamental Research Funds for the Central Universities (Grant No. N110202001).

References

Akimoto, S. and Katsura, T. 1959. Magnetochemical study of the generalized titanomagnetic in volcanic rocks. *Journal of Geomagnetism and Geoelectricity*, vol. 10. pp. 69–90.

Barksdale, J. 1966. Titanium, its Chemistry and Technology. 2nd edn, Roland Press, New York.

Chen, D.S., Song, B., and Wang, L.N. 2011. Solid state reduction of Panzhihua titanomagnetite concentrates with pulverized coal. *Minerals Engineering*, vol. 24, no. 8. pp. 864–869.

Diao, R.S. 1999. New understanding about special problems of smelting vanadium-bearing titanomagnetite with BF. *Iron and Steel*, vol. 34, no. 6. pp. 12–14.

Huang, X.H. 2007. Ferrous Metallurgy Theory. Metallurgical Industry Press, Beijing. pp. 268–277.

Katsura, T. and Kushiro, I. 1961. Titanomagnetic in igneous rocks. *American Mineralogist*, vol. 46. pp. 134–145.

Lei, Y., Li, Y., and Peng, J.H. 2011. Carbothermic reduction of Panzhihua oxidized ilmenite in a microwave field. *ISIJ International*, vol. 51, no. 3. pp. 337–343.

Ma, J.Y., Sun, X.W., and Sheng, S.X. 2000. Intensified smelting of vanadium and titanium magnetite in blast furnace. *Iron and Steel*, vol. 35, no. 1. pp. 4–8.

Paunova, R. 2002. Thermodynamic study of the reduction of titanium magnetite concentrate with solid carbon. *Metallurgical and Materials Transactions B*, vol. 33, no. 8. pp. 633–638.

Pesl, J. and Eric, R.H. 2002. High temperature carbothermic reduction of Fe_2O_3-TiO_2-M_xO_y oxide mixtures. *Minerals Engineering*, vol. 15. pp. 971–984.

Pogudin, D.S., Morozov, A.A., and Sadykhov, G.B. 2010. Phase formation during the reduction of titanomagnetite from the Gremyakha-Vyrmes deposit. *Russian Metallurgy*, vol. 9. pp. 759–762.

Roshchin, V.E., Asanov, A.V., and Roshchin A.V. 2011. Possibilities of two-stage processing of titaniferous magnetite ore concentrates. *Russian Metallurgy*, vol. 6. pp. 15–25.

Sadykhov, G.B., Goncharov, K.V., and Goncharenko, T.V. 2010. Phase composition of the vanadium-containing titanium slags forming upon the reduction smelting of the titanomagnetite concentrate from the Kuranakhsk deposit. *Russian Metallurgy*, vol. 7. pp. 581–587.

Wang, Y.M., Yuan, Z F., and Guo, Z.C. 2008. Reduction mechanism of natural ilmenite with graphite. *Transactions of the Nonferrous Metals Society*, vol. 18, no. 4. pp. 962–968.

Welham, N.J. 1996. A parametric study of the mechanically activated carbothermic reduction of ilmentite. *Minerals Engineering*, vol. 9. pp. 1189–1200.

Yuan, Z.F., Wang, X.Q., and Xu, C. 2006. A new process for comprehensive utilization of complex titania ore. *Minerals Engineering*, vol. 19, no. 11. pp. 975–978. ◆